19

Analysis of optical properties of disordered array of hemispherical Ag nanoparticles on SiO_2/c-Si by spectroscopic ellipsometry

© A.A. Ermina, V.O. Bolshakov, K.V. Prigoda, V.A. Tolmachev, S.A. Grudinkin, Yu.A. Zharova¶

Ioffe Institute,
St. Petersburg, Russia

¶ e-mail: piliouguina@mail.ioffe.ru

Received May 02, 2024
Revised May 26, 2024
Accepted July 05, 2024

In this work, a disordered array of self-organized hemispherical Ag nanoparticles on a SiO_2/Si surface was studied. The structures were obtained by a simple, reproducible and low-cost method based on the reduction of Ag from solution on the silicon surface, followed by annealing in an O_2 atmosphere at 350°C. Experimental data are analyzed using the Bruggeman effective medium approximation and Lorentz oscillators which determined the volume fraction of Ag and plasmon resonances positions, respectively. The numerical spectral positions of localized surface plasmon resonances are in good agreement with the data obtained by spectroscopic ellipsometry.

Keywords: hemispherical Ag nanoparticles, single-crystal silicon, localized surface plasmon resonance, spectroscopic ellipsometry, effective medium approximation.

DOI: 10.61011/EOS.2024.07.59652.6515-24

Introduction

Localized surface plasmon resonance (LSPR) that occurs in metallic nanostructures during interaction between light and free metal electrons provides dramatic increase in the electromagnetic field on nanoscale structure surfaces [1]. Interest in the study of LSPR structures is growing from year to year due to a high potential of plasmon nanostructures in many applications, including photovoltaics [2,3], nanoplasmonic sensorics [4,5], surface-enhanced Raman spectroscopy (SERS) [6,7] and nonlinear optics [8,9]. To control the position of the LSPR, researchers use various substrates [6,10], noble metals (Au, Ag, Pt and combinations thereof) [6] and various metallic nanoparticle synthesis techniques [6,11,12] through modification of the optical properties of structures by varying nanoparticle sizes and shapes, interparticle distances and interactions, and environment permittivity [1,13–15]. For characterization of the optical structures of plasmon nanostructures, their complex permittivity ($\varepsilon = \varepsilon_1 + i\varepsilon_2$, where ε_1 is the real part and ε_2 is the imaginary part), that combines the electric field response in reflection or transmission, shall be determined. There are two standard methods for determining the permittivity of a material: (1) reflectance and transmission spectroscopy, (2) spectroscopic ellipsometry. Reflectance and transmission spectroscopy measures the reflected and transmitted intensity after interaction with a material. By combining these reflections and transmissions, the permittivity may be determined. If a material is nontransparent in this measurement range, then only one of the measurements (reflection) is available, and the Kramers–Kronig theorem is used to determine the permittivity. However, there is often a related uncertainty in the real part value ε_1. The advantage of the spectroscopic ellipsometry, in this case, is in simultaneous measurement of both amplitude ratio and phase difference of orthogonally polarized light. This provides two measured parameters that are used to calculate the real and imaginary part of permittivity and to avoid using the Kramers–Kronig analysis [16]. Experimental data obtained by multi-angle spectroscopic ellipsometry method are analyzed using the Bruggeman effective medium approximation to determine the volume fraction (filling factor) of metal [17], the Drude model to describe free electrons [18], the Tanguy model [19] to describe the interband transition effect, and the Lorentz model [20,21], the Gaussian model [22,23] or combination thereof [24] to describe plasmon resonances. In this work, the plasmonic properties of hemispherical silver nanoparticles synthesized by chemical deposition followed by annealing in an O_2 atmosphere were investigated. This method features low cost compared with magnetron, ion-beam or electronic sputtering methods that require expensive equipment and chemicals. The surface morphology was studied by the scanning electron microscopy method. The multi-angle spectroscopic ellipsometry was used to study optical (plasmonic) properties of nanostructures. Pseudo-permittivities ($\langle\varepsilon\rangle = \langle\varepsilon_1\rangle + i\langle\varepsilon_2\rangle$) of hemispherical silver nanoparticles on SiO_2/c-Si were determined. Pseudo-permittivity is used to describe the optical properties of composite structures or structures without smooth (parallel) interface with medium (air) [25].

1. Experimental procedure

1.1. Material and nanostructure fabrication technique

Wafers of *p*-type (boron doped) single-crystal silicon (*c*-Si) with $\rho = 10\,\Omega \times \text{cm}$ and crystallographic orientation (100) were used as substrates. Island Ag films were grown in the Volmer–Weber mode on the surface of clean c-Si wafers by the chemical deposition method ($0.02\,\text{M}\,AgNO_3 + 5\,\text{M}\,HF$, in volume ratio 1:2, 1:4, 1:6, 1:8, during 30 s). As a result of such deposition, the island Ag films differed from each other in morphology due to different solution concentrations [26]. Then these films were annealed in O_2 at 350°C during 30 min. Finally, disordered array of hemispherical Ag nanoparticles (AgNPs) of different sizes were produced depending on the initial Ag island film morphology.

1.2. Nanostructure characterization methods

Scanning electron microscopy (SEM). The morphology of nanostructures was studied in the secondary electron mode at an accelerating voltage of 5 kV using the SUPRA 55VP-25–78 (Zeiss, Germany) scanning-electron microscope. The statistical analysis of nanostructures (average size, filling factor and distance between nanoparticles) was performed using SEM images and ImageJ open source software. The interparticle distances were determined by the center-to-center distance („Center of mass" in ImageJ measurement settings) of two nearby AgNPs.

Spectroscopic ellipsometry (SE). Ellipsometric properties were examined using the SE-2000 (Semilab, Hungary) spectroscopic ellipsometer in the wavelength range λ from 270 nm to 900 nm at the incidence angles φ from 45° to 70° at 5°intervals. Two ellipsometric angles Ψ and Δ are measured simultaneously, where $\Psi = \text{arctg}(|R_p|/|R_s|)$ and $\Delta = \arg(R_p/R_s) = \delta R_p - \delta R_s$ is the phase difference, R_p, R_s are complex reflection coefficients for p- and s-polarized light. The basic reflection ellipsometry equation is written as:

$$\rho = R_p/R_s = \text{tg}(\Psi)e^{i\Delta}, \quad (1)$$

where ρ is the system's relative reflection coefficient. Complex pseudo-permittivity is calculated as:

$$\langle\varepsilon_1\rangle = \langle\varepsilon_1\rangle + i\langle\varepsilon_2\rangle = \sin^2(\varphi)\left[1 + \frac{(1-\rho)^2}{(1+\rho)^2}\tan^2(\varphi)\right]. \quad (2)$$

2. Results

2.1. Morphologies of obtaned structures

For the purpose of this study, annealing of the Ag island film was performed at 350°C during 30 min in O_2. After such annealing, the island film transforms into a disordered array of stand-alone hemispherical nanoparticles of different sizes, the morphology of which is shown in Figure 1. The analysis of SEM images is shown in Table 1.

According to the SE data, thickness of the SiO_2 layer on the c-Si substrate is maximum 5 nm. Annealing at higher temperatures leads to an increase the growth rate of SiO_2 and the covering of AgNPs with SiO_2 it as shown in [27].

2.2. Optical properties of nanostructures

The results of the SE investigation of the complex permittivity and pseudo-permittivity of Ag island films on the c-Si surface are shown in [28–30]. Ag island films with a layer thickness of from 45 nm to 50 nm in the complex permittivity spectra exhibit a resonance feature — longitudinal-mode plasmon resonance ($E = 3.8$ eV), and the complex pseudo-permittivity $\langle\varepsilon\rangle$ is close to that of „bulk" Ag [16].

In this study, the complex pseudo-permittivity of the disordered array of hemispherical AgNPs on the SiO_2/c-Si surface obtained after annealing of the initial Ag island films is considered. Note that spectral dependence of the real and imaginary parts $\langle\varepsilon\rangle$ varies negligibly depending on the incidence angle for all studied samples. Figure 2 shows the real and imaginary parts $\langle\varepsilon\rangle$ of the 1:6 sample (as an example) for six incidence angles. As the incidence angle decreases from 70° to 45°, small noise appears in the spectra, that is why an angle of 70° is chosen for further spectra analysis demonstration.

Figure 3 shows experimental spectra of the real and imaginary parts $\langle\varepsilon\rangle$ as dotted and dashed lines for all studied samples. In the wavelength range of 310–332 nm, singularities associated with interband transition in Ag and appearance of the "bulk" plasmon resonance of Ag are observed. The influence of the interband transition in Ag and the „bulk" plasmon resonance of Ag on each other does not allow us to determine their positions, since the interband transition in Ag corresponds to an energy of 4–4.1 eV (300–310 nm) [31], and the position of the „bulk" plasmon resonance of Ag is about 3.8–3.9 eV (318–326 nm). At the same time, the $\langle\varepsilon_2\rangle$ spectra display peaks at 657 nm, 671 nm, 714 nm and 754 nm corresponding to the appearance of the LSPR dipole mode associated with scattering [26]. The larger the nanoparticles the larger the shift to the red visible range.

The experimental spectra were examined using the Bruggeman effective medium approximation to determine the filling factor and AgNPs layer thickness, wherein the permittivity of Ag was set using the Drude and Lorentz dispersion models. We have also considered geometries of the studied structures by using a multilayer model with parabolic Ag/air gradient (Figure 4, *a*). This model consists of a semi-infinite silicon substrate, SiO_2 layer and composite Ag/air layer. To ensure the best convergence of calculated spectra to the experimental ones, the model used 22 Ag/air layers for the 1:2 and 1:4 samples, 10 layers for the 1:6 sample and 14 layers for the 1:8 sample. The models are discussed in detail below.

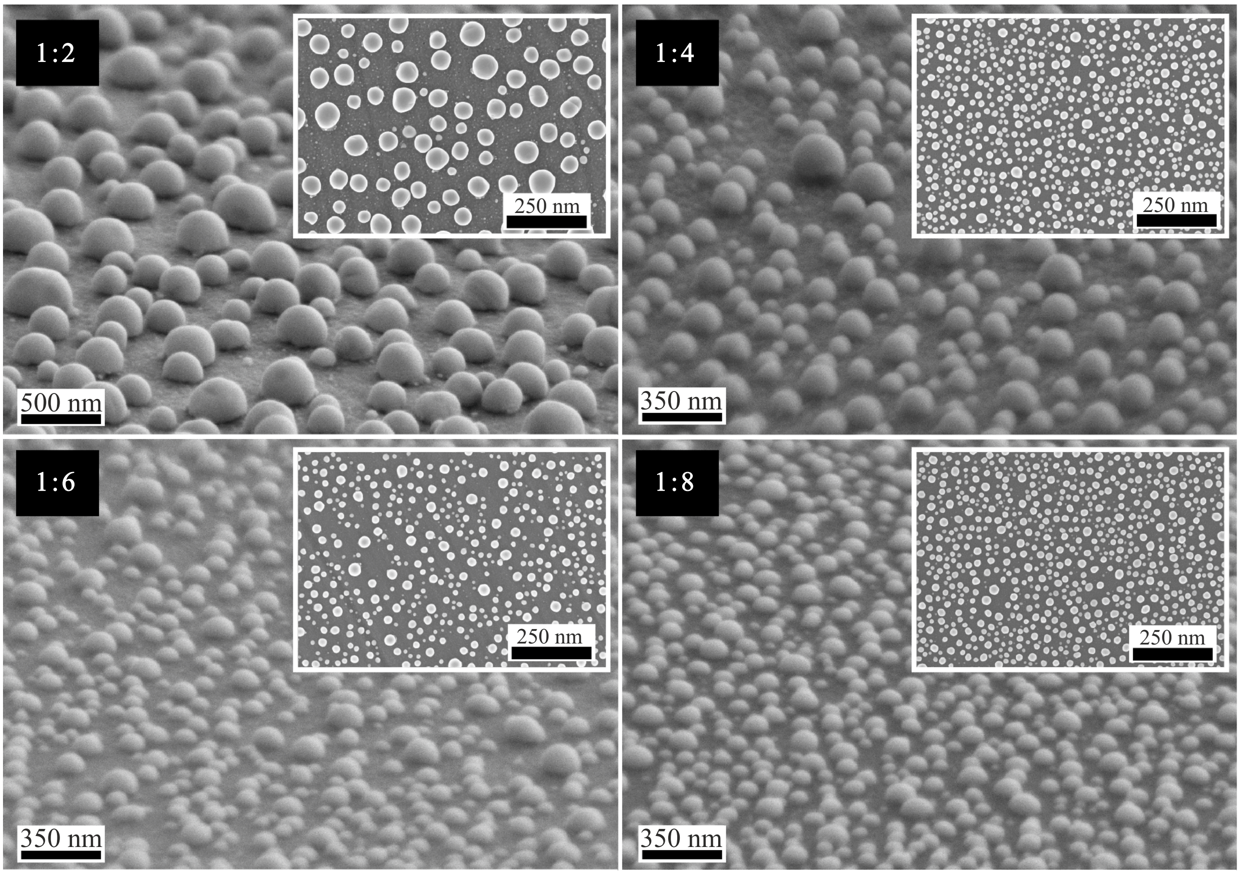

Figure 1. SEM images of nanostructures (isometric view) obtained at various solution concentrations from 1:2 to 1:8. The insets show SEM images (top view) of the corresponding samples.

Table 1. Morphological parameters of hemispherical AgNPs on SiO_2/c-Si

Volume ratio of 0.02 M $AgNO_3$ and 5 M HF	1:2	1:4	1:6	1:8
r, nm	87 ± 21	56 ± 19	41 ± 14	32 ± 11
Interparticle distance, nm	213 ± 58	144 ± 41	100 ± 20	81 ± 16
Filling factor, %	32	34	37	38
h, nm	108 ± 22	72 ± 17	50 ± 11	39 ± 10

2.2.1. Bruggeman effective medium approximation

The filling factor of Ag in each Ag/air layer was determined using the effective medium approximation:

$$f_1 \frac{\langle \varepsilon \rangle - \varepsilon_1}{\varepsilon_1 + 2\langle \varepsilon \rangle} + f_2 \frac{\langle \varepsilon \rangle - \varepsilon_2}{\varepsilon_2 + 2\langle \varepsilon \rangle} = 0, \quad (3)$$

where $\langle \varepsilon \rangle$ is the effective permittivity of the composite material, ε_1, ε_2 are the permittivities of Ag and air, f_1, f_2 are the filling factors of Ag and air, respectively. Distribution of the filling factor of Ag in air was defined by the parabolic gradient using equation (4), since such dependence adequately describes the shape of the experimental hemispherical AgNP.

$$f_i = a\left(\frac{h_i - h_0}{h_{\text{calc}}}\right)^2 + c_0, \quad (4)$$

where f_i is the filling factor of Ag in air, h_i is the n-th Ag layer position (Figure 4, a) for which the filling factor is specified, c_0, a, h_0 are the coefficients defining the parabola shape and position, h_{calc} is the calculated effective thickness of the Ag layer. Values of a are negative because the air/Ag filling factor decreases as the nanostructure height increases.

Figure 4, b shows the dependence of the filling factor of Ag on the Ag/air layer height where the parabolic function parameters (a, h_0, c_0) for each sample are taken from Table 2. Thus, the numeric filling factors of the first Ag/air layer for the 1:2, 1:4, 1:6 and 1:8 samples are equal to 41%, 44%, 36% and 42%, respectively. For the effective medium approximation, there are object size limits (atomic size $\ll h < \lambda/10$) [25]. Note that there is good convergence of experimental AgNPs heights measured by the SEM

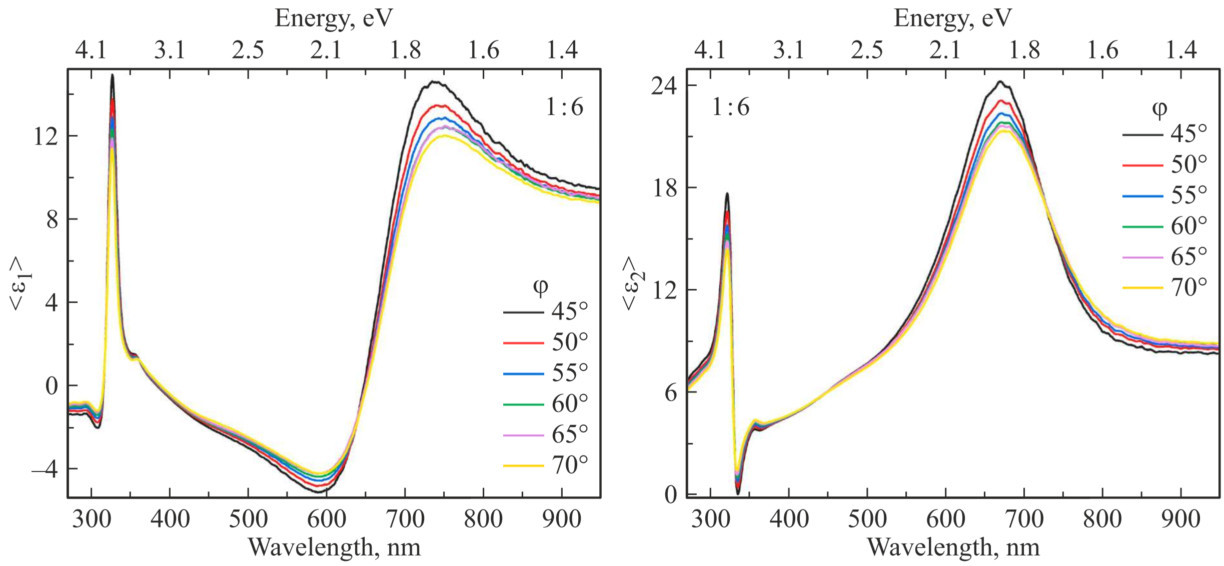

Figure 2. Spectral dependences of the real $\langle\varepsilon_1\rangle$ and imaginary $\langle\varepsilon_2\rangle$ parts of the pseudo-permittivity on different incidence angles for the 1:6 sample.

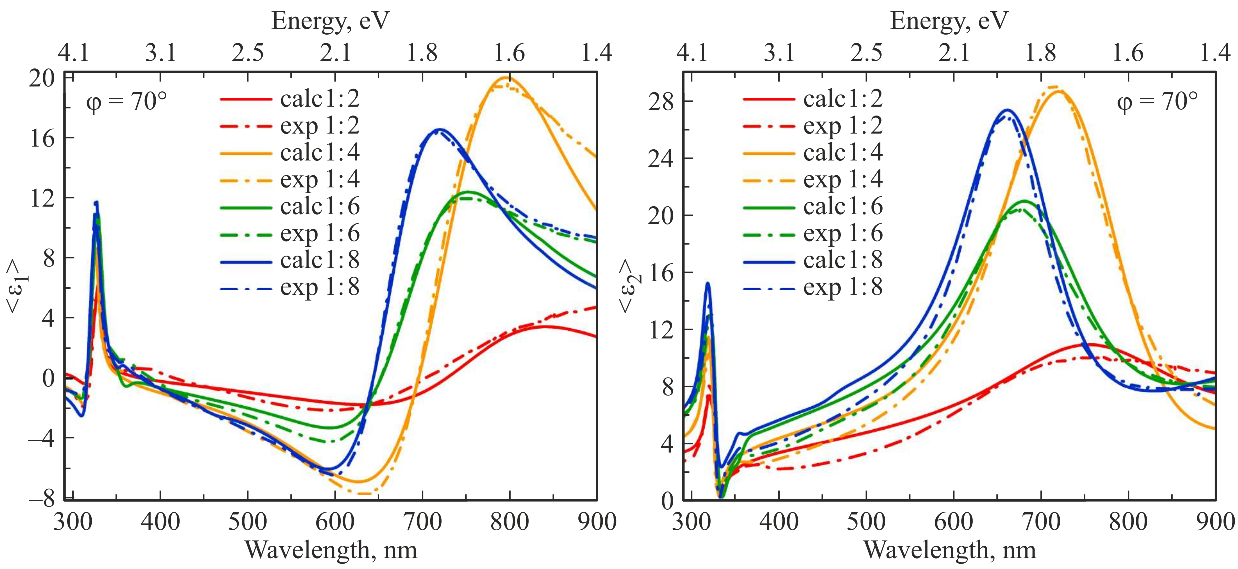

Figure 3. Spectral dependences of the real $\langle\varepsilon_1\rangle$ and imaginary $\langle\varepsilon_2\rangle$ parts of pseudo-permittivity at $\varphi = 70^\circ$ for the 1:2 (red line), 1:4 (orange line), 1:6 (green line), 1:8 (blue line) samples, where the dash-dotted lines indicate the experimental data and the solid lines indicate approximation.

method and the SiO_2 layer thickness measured by the SE method with the calculated effective thicknesses (Table 2), including for the 1:2 and 1:4 samples, notwithstanding the AgNP heights.

2.2.2. Drude model

The Drude model is necessary to describe the optical properties associated with light absorption by free electrons and is written as:

$$\varepsilon_1 = 1 - \frac{(E_P/E)^2}{1 + (E_\Gamma/E)^2}, \tag{5}$$

$$\varepsilon_2 = \frac{E_\Gamma (E_P/E)^2}{E(1 + (E_\Gamma/E)^2)}, \tag{6}$$

where E_P and E_Γ are the plasma and damping energies associated with the scattering frequency, respectively [32]. For our case $E_P = 8.6$ eV and $E_\Gamma = 0.07$ eV for all samples. E is the incident light energy.

2.2.3. Lorentz model

This model is a harmonic dipole oscillator. In this case, two Lorentz oscillators were used in each Ag/air layer. To describe the plasmon resonances, the following real and

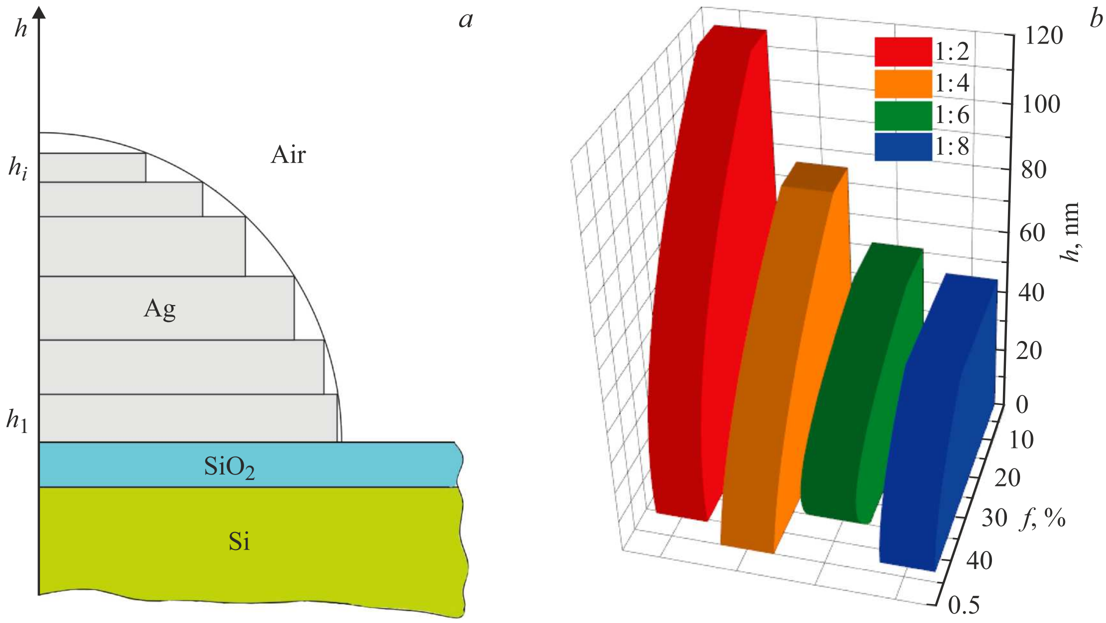

Figure 4. (*a*) Schematic multilayer model consisting of the semi-infinite silicon substrate, SiO_2 layer and Ag/air layer with the parabolic gradient; (*b*) dependence of the height (h) of the Ag/air layer on the filling factor (f) of Ag for each sample, where the parabolic function parameters (a, h_0, c_0) are taken from Table 2.

Table 2. Parameters obtained using the Bruggeman effective medium approximation for each sample

Sample	Layer		a	h_0, nm	c_0	h_{calc}, nm	h_{exp}, nm
1:2	1	SiO_2		–		5	5
	2	Air/Ag	-0.32	0	0.43	105	108 ± 22
1:4	1	SiO_2		–		5	5
	2	Air/Ag	-0.27	-15	0.46	75	72 ± 17
1:6	1	SiO_2		–		5	5
	2	Air/Ag	-0.69	16.9	0.42	51	50 ± 11
1:8	1	SiO_2		–		8.5	5
	2	Air/Ag	-0.19	2.8	0.43	44	39 ± 10

imaginary parts of permittivity are used:

$$\varepsilon_1 = \frac{FE_0^2(E_0^2 - E^2)}{(E_0^2 - E^2)^2 + \Gamma^2 E^2}, \tag{7}$$

$$\varepsilon_2 = \frac{FE_0^2 \Gamma E}{(E_0^2 - E^2)^2 + \Gamma^2 E^2}, \tag{8}$$

where F is the amplitude, E_0 is the position, Γ is the oscillator damping [32].

Table 3 shows the fitted Lorentz model parameters for each sample. As a result of approximation, the calculated (solid lines) and experimental (dash-dotted lines) spectra (Figure 3) have quite good convergence, and RMSE for the 1:2 sample is 0.81, for the 1:4 sample is 1.14, for the 1:6 sample is 0.8 and for the 1:8 sample is 1.12. The Lorentz peaks at 3.87 eV and 3.9 eV describe the „bulk" plasmon resonance of Ag, and the peaks at 1.65 eV, 1.71 eV, 1.85 eV and 1.87 eV describe LSPR, which tends to shift to the red spectrum range. This shift is associated with the increase in AgNPs sizes. The damping energy is inversely proportional to the resonance Q-factor. The larger the damping energy the wider the resonance.

Conclusion

In this work, the plasmonic properties of a disordered array of hemispherical AgNPs of different morphologies on the SiO_2/c-Si substrate using the multi-angle spectroscopic ellipsometry method were studied.

Table 3. Calculated Lorentz model parameters for each sample

Sample	F	E_0, eV	$\hbar\Gamma$, eV
1:2	1.35 21.6	3.87 1.65	0.13 0.64
1:4	2.31 45.22	3.9 1.71	0.18 0.5
1:6	5.1 39.79	3.9 1.85	0.19 0.48
1:8	4.46 33.28	3.9 1.87	0.24 0.43

The structures were obtained on the c-Si surface using the chemical deposition method from a solution with different $AgNO_3$ concentrations and then annealed at 350°C in O_2. The average radius of AgNP varied from 30 nm to 90 nm, the filling factor varied from 38% to 32% depending on the solution concentration. The considered method is quite simple and does not require expensive equipment and chemicals.

Using the spectroscopic ellipsometry and the Bruggeman effective medium approximation, Drude and Lorentz models, good convergence between the experimental and calculated pseudo-permittivity spectra with RMSE of about 1 was achieved.

Thus, the fundamental studies described in this work may be useful for studying the optical properties of nanostructures on an opaque substrate when it is impossible to measure transmission and obtain absorption.

Funding

The study was supported by the Ministry of Science and Higher Education of the Russian Federation under the state assignment (project № FFUG-2024-0017).

Acknowledgment

The authors are grateful to Oleg Medvedev for SEM investigation.

Conflict of interest

The authors declare that they have no conflict of interest.

References

[1] S.A. Maier. *Plasmonics: Fundamentals and Applications*, 1st ed. (Springer New York, NY, 2007). DOI: 10.1007/0-387-37825-1
[2] Y.H. Jang, Y.J. Jang, S. Kim, L.N. Quan, K. Chung, D.H. Kim. Chem. Rev., **116** (24), 14982 (2016). DOI: 10.1021/acs.chemrev.6b00302
[3] H.A. Atwater, A. Polman. Nat. Mater., **9**, 205 (2010). DOI: 10.1038/nmat2629
[4] M. Pan, J. Yang, K. Liu, Z. Yin, T. Ma, S. Liu, L. Xu, S. Wang. Nanomat., **10** (2), 209 (2020). DOI: 10.3390/nano10020209
[5] I. Shutsko, M. Buchmüller, M. Meudt, P. Görrn. Adv. Opt. Mater., **10** (9), 2102783 (2022). DOI: 10.1002/adom.202102783
[6] B. Sharma, R.R. Frontiera, A.-I. Henry, E. Ringe, R.P. Van Duyne. Mat. Tod., **15** (1−2), 16 (2012). DOI: 10.1016/S1369-7021(12)70017-2
[7] J. Langer et al. ACS Nano, **14** (1), 28 (2020). DOI: 10.1021/acsnano.9b04224
[8] M. Lippitz, M.A. Van Dijk, M. Orrit. Nano Lett., **5** (4), 799 (2005). DOI: 10.1021/nl0502571
[9] Z.-W. Yang, L.-Y. Meng, J.-S. Lin, W.-M. Yang, P. Radjenovic, S.-X. Shen, Q.-C. Xu, Z.-L. Yang, Z.-Q. Tian, J.-F. Li. Adv. Opt. Mater., **7** (23), 1901010 (2019). DOI: 10.1002/adom.201901010
[10] J.-A. Huang, Y.-L. Zhang, H. Ding, H.-B. Sun. Adv. Opt. Mater., **3** (5), 618 (2015). DOI: 10.1002/adom.201400534
[11] K. Rhee, A. Tukova, M.T. Yaraki, Y. Wang. Nanoscale, **15** (5), 2087 (2023). DOI: 10.1039/D2NR05287C
[12] A. Das, U. Pant, C. Cao, R.S. Moirangthem, H.B. Kamble. Nano Res., **16**, 1132 (2023). DOI: 10.1007/s12274-022-4745-0
[13] X. Lu, M. Rycenga, S.E. Skrabalak, B. Wiley, Y. Xia. Annu. Rev. Phys. Chem., **60**, 167 (2009). DOI: 10.1146/annurev.physchem.040808.090434
[14] S. Szunerits, M.R. Das, R. Boukherroub. J. Phys. Chem. C., **112** (22), 8239 (2008). DOI: 10.1021/jp800478h
[15] W.J. Ho, S.K. Fen, J.J. Liu. Appl. Phys. A., **124**, 29 (2018). DOI: 10.1007/s00339-017-1451-y
[16] T.W.H. Oates, H. Wormeester, H. Arwin. Prog. Surf. Sci., **86** (11−12), 328 (2011). DOI: 10.1016/j.progsurf.2011.08.004
[17] D.A.G. Bruggeman. Ann. Phys., **416**, 636 (1935). DOI: 10.1002/andp.19354160705
[18] P. Drude. Ann. Phys., **270** (7), 489 (1888). DOI: 10.1002/andp.18882700706
[19] C. Tanguy. Phys. Rev. B, **60** (15), 10660 (1999). DOI: 10.1103/PhysRevB.60.10660
[20] M. Voué, N. Dahmouchene, J. De Coninck. Thin Solid Films, **519** (9), 2963 (2011).
[21] A. Baron, A. Iazzolino, K. Ehrhardt, J.-B. Salmon, A. Aradian, V. Kravets, A.N. Grigorenko, J. Leng, A. Le Beulze, M. Tréguer-Delapierre, M.A. Correa-Duarte, P. Barois. Opt. Mater. Express, **3** (11), 1792 (2013). DOI: 10.1364/OME.3.001792
[22] M. Lončarić, J. Sancho-Parramon, H. Zorc. Thin Solid Films, **519** (9), 2946 (2011). DOI: 10.1016/j.tsf.2010.12.06
[23] M.N. Perera, D. Schmidt, W.E.K. Gibbs, S. Juodkazis, P.R. Stoddart. Opt. Lett., **41** (23), 5495 (2016). DOI: 10.1364/OL.41.005495
[24] M.S. Gangwar, P. Agarwal. Phys. Scr., **98** (10), 105944 (2023). DOI: 10.1088/1402-4896/acf796
[25] H. Fujiwara. *Spectroscopic ellipsometry: principles and applications*, 1st ed (John Wiley & Sons, Hoboken, USA, 2007).
[26] A.A. Ermina, N.S. Solodovchenko, V.S. Levitskii, N.A. Belskaya, S.I. Pavlov, V.O. Bolshakov, V.A. Tolmachev, Yu.A. Zharova. Mater. Sci. Semicond. Process., **169**, 107861 (2024). DOI: 10.1016/j.mssp.2023.107861
[27] A.A. Ermina, N.S. Solodovchenko, K.V. Prigoda, V.S. Levitskii, V.O. Bolshakov, M.Yu. Maximov, Y.M. Koshtyal,

S.I. Pavlov, V.A. Tolmachev, Y.A. Zharova. Appl. Surf. Sci., **608**, 155146 (2023). DOI: 10.1016/j.apsusc.2022.155146
[28] V.A. Tolmachev, E.V. Gushchina, I.A. Nyapshaev, Yu.A. Zharova. Thin Solid Films, **756**, 139352 (2022). DOI: 10.1016/j.tsf.2022.139352
[29] Y. Zharova, A. Ermina, S. Pavlov, Y. Koshtyal, V. Tolmachev. Phys. Status Solidi A, **216** (17), 1900318 (2019). DOI: 10.1002/pssa.201900318
[30] V.A. Tolmachev, Y.A. Zharova, A.A. Ermina, V.O. Bolshakov. Opt. Spectr., **130** (2), 238 (2022). DOI: 10.21883/EOS.2022.02.53215.2668-21.
[31] U. Kreibig, M. Vollmer. *Optical Properties of Metal Clusters*, 1st ed (Springer Berlin, Heidelberg, 1995). DOI: 10.1007/978-3-662-09109-8
[32] *Handbook of ellipsometry*, ed. by H.G. Tompkins, E.A. Irene (William Andrew Pub., Norwich and Springer, Heidelberg, 2005).

Translated by E.Ilinskaya